On the Nature and Elimination of Stimulus Artifact in Nerve Signals Evoked and Recorded Using Surface Electrodes

KEVIN C. McGILL, KENNETH L. CUMMINS, MEMBER, IEEE, LESLIE J. DORFMAN, BRUNO B. BERLIZOT, KELLY LUETKEMEYER, DWIGHT G. NISHIMURA, AND BERNARD WIDROW, FELLOW, IEEE

Abstract—**The electrical stimulus pulse and the surface electrodes commonly used to study compound action potentials of peripheral nerves give rise to an artifact consisting of an initial spike and a longer lasting tail which often interferes with the recorded signal. The artifact has four sources: 1) the voltage gradient between the recording electrodes caused by stimulus current flowing through the limb, 2) the common-mode voltage of the limb caused by current escaping through the ground electrode, 3) the capacitive coupling between the stimulating and recording leads, and 4) the high-pass filtering characteristics of the recording amplifier. This paper models these sources and presents several methodological rules for minimizing their effects. Also presented are three computer-based methods for subtracting the residual artifact from contaminated records using estimates of the artifact obtained from: 1) subthreshold stimulation, 2) a second recording site remote from the nerve, or 3) stimulation during the refractory period of the nerve.**

I. INTRODUCTION

A widely used technique for measuring the compound action potential (CAP) of a peripheral nerve employs surface electrodes to stimulate the nerve and record the signal. The recorded signal is often contaminated by stimulus artifact. While this artifact does not usually hamper simple analysis of the CAP, such as measurement of the latency to peak, it does interfere with analysis which requires accurate knowledge of the CAP waveform, such as estimation of the distribution of fiber conduction velocities (DCV). This paper presents and explains by theoretical models several rules for reducing stimulus artifact and several methods for extracting the CAP from a contaminated record.

A typical configuration for measuring the mixed motor/sensory CAP of the median nerve is shown in Fig. 1(a). The nerve is stimulated at the wrist by a rectangular pulse of current. Sharp supramaximal stimulation requires a pulse of 0.1-0.2 ms in duration and up to 60 mA in intensity. The nerve signal is recorded differentially between an electrode positioned over the nerve at the elbow and an indifferent electrode 2-5 cm away. The limb is grounded by an electrode between the stimulating and recording sites to reduce 60-Hz interference, to hold the mean voltage of the limb near ground, and to prevent transthoracic current flow if a failure shorts one of the stimulator leads to supply voltage or ground. To ensure good consistent electrical contact, the skin is mildly abraded and electrolyte paste is applied under each electrode. All of the measurements reported in this paper were made with stainless steel disk electrodes, 1 cm in diameter for stimulating and recording, 3.2 cm in diameter for grounding.

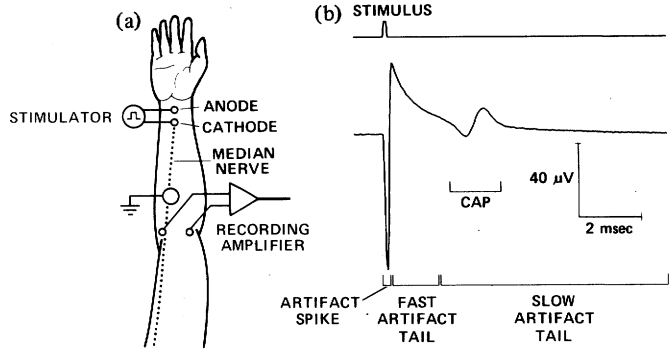

Fig. 1. (a) Electrode configuration for measuring the mixed motor/sensory compound action potential (CAP) of the median nerve. (b) A recorded CAP contaminated by artifact.

A typical contaminated CAP record is shown in Fig. 1(b). The biphasic nerve signal is 20 μV p-p and begins 2 ms after the stimulus. The artifact has three parts: a spike coincident with the stimulus pulse and many times larger than the nerve signal, a fast-tail component, and a slow-tail component.

II. THE COMPONENTS AND THEIR ELECTRICAL PROPERTIES

An electrical model for explaining artifact must take into account the stimulator, the electrode/skin interfaces, the subcutaneous tissue of the limb, and the recording amplifier. Each of these components will now be discussed.

A. Stimulator

The two characteristics of the stimulator which affect artifact are the type of stimulation (constant-voltage or constant-current) and the capacitance to ground. Related to the type of stimulation is the output impedance of the stimulator: a constant-voltage stimulator has a low output impedance

Manuscript received April 28, 1981; revised September 18, 1981. This work was supported by a grant from the Muscular Dystrophy Association (LJD), and by the National Science Foundation under Grant ECS-7808526 (BW).

K. C. McGill, D. G. Nishimura, and B. Widrow are with the Department of Electrical Engineering, Stanford University, Stanford, CA 94305.

K. L. Cummins is with the Rehabilitative Engineering Research and Development (RERanD) Center, Palo Alto Veterans Administration Medical Center, Palo Alto, CA 94305.

L. J. Dorfman is with the Department of Neurology, Stanford University Medical Center, Stanford, CA 94305.

B. B. Berlizot was with the Department of Electrical Engineering, Stanford University, Stanford, CA 94305. He is now with Services Informatiques Logiciels et Etudes-Siloé, Saint-Tropez, France.

K. Luetkemeyer was with the Department of Electrical Engineering, Stanford University, Stanford, CA 94305. He is now with NASA Ames Research Center, Moffett Field, CA 94305.

0018-9294/82/0200-0129$00.75

(<1 kΩ), a constant-current stimulator has a high output impedance (>100 kΩ).

The stimulator outputs must float with respect to ground to allow the ground electrode to fix the potential of the limb. Floating is accomplished by transformer-coupling the pulse or by electrically isolating the entire pulse generator. In either case, stray capacitances to ground exist. The stray capacitances of a transformer-coupled stimulator can be modeled as lumped capacitors, typically 100-200 pF, between each output and ground. Modeling electrically isolated and constant-current stimulators is more complicated since active components separate the stray capacitances from the output terminals. Guld [1] and Neilson [2] have proposed shielding schemes to reduce the effective capacitance between the outputs and ground, but most commercial stimulators are not so shielded.

B. Electrode/Skin Interface

The interface between the surface electrode and the subcutaneous tissue is complex and incompletely understood. This section briefly discusses the two major components of the interface—the metal/electrolyte junction and the skin—and presents simple electrical models for the interface at low and high current densities.

The junction between metal electrode and electrolyte paste has been widely studied and modeled [3]-[11]. Metal atoms dissociate into the electrolyte and form a double-charge layer which is responsible for the dc half-cell potential, the large electrolytic capacitance between metal and solution, and the parallel frequency- and current-density-dependent polarization capacitance. Direct current crosses the interface via electrochemical reactions in which electrons in the metal are exchanged for ions in solution, and the resulting voltage drop is nonlinearly related to the current. For a pair of stainless steel electrodes 1 cm in diameter in contact with EKG-Sol paste (Burton, Parsons & Co.), the difference in half-cell potentials is typically several tenths of a volt, the net capacitance is about 50 μF, and the effective resistance is several kilohms.

The outer layers of the skin—the keratinous layer and the epidermis—form a resistive sheath around the conductive tissue within [3], [4], [12]-[14]. The resistance of these layers decreases with increasing current density and is reduced by abrasion, by the application of electrolyte paste, and by the activity of the sweat glands. Variations in skin resistance caused by sweating and by irregular contact due to bodily hair are reduced by electrolyte paste. Ionic processes in the skin give rise to the galvanic skin potential and to electrolytic and polarization capacitances between the surface and the subcutaneous tissue. The resistance of the skin under a 1 cm diameter electrode ranges from 100 kΩ for unprepared skin to 10 kΩ or less for mildly abraded skin, while the capacitance is about 0.03 μF regardless of preparation.

At the low current densities conducted by the recording and ground electrodes, the electrode interface is dominated by the impedance of the skin and can be modeled by a fixed resistor in parallel with a fixed capacitor, as verified empirically by several investigators [3]-[5], [8]. This model ignores the electrode's half-cell potential and the galvanic skin potential which are blocked by the recording amplifier's high-pass filter.

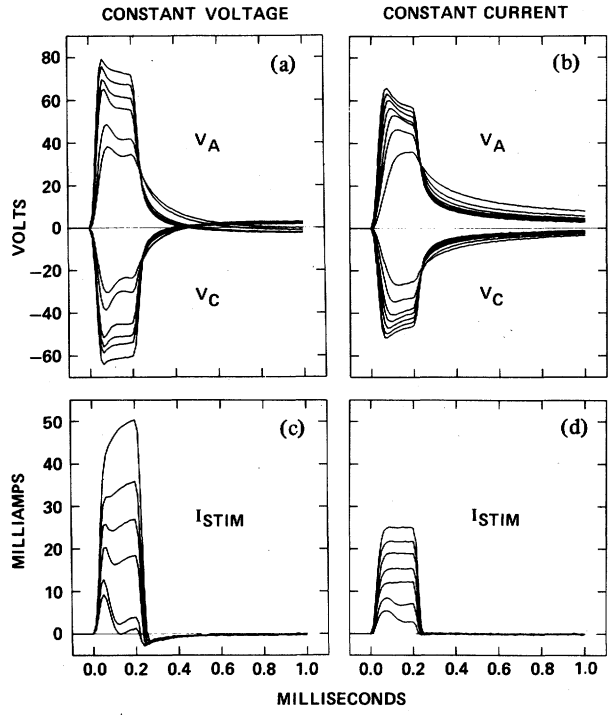

Fig. 2. Nonlinear current/voltage characteristics of the stimulating electrodes. Constant-voltage pulses give rise to the anode and cathode voltages shown in (a) and the currents shown in (c). Constant-current pulses (d) give rise to the anode and cathode voltages shown in (b).

At the high current densities conducted by the stimulating electrodes, the electrode interface is more complicated. Fig. 2 shows the voltages of the anode (V_A) and cathode (V_C) with respect to ground and the current (I_{stim}) during pulses of constant voltage and constant current applied through new electrodes at the wrist, which had been wiped with alcohol, but not abraded. Notice that the anode voltage is larger than the cathode voltage. This is due to intrinsic differences in skin impedance at the wrist, rather than polarity of current flow. Nonlinearity can be seen in Fig. 2 in the relationship between peak values of voltage and current and in the nonexponential relaxations. Notice that current continues to flow after the falling edge of a constant-voltage pulse as the skin capacitance discharges through the low output impedance of the stimulator. After a constant-current pulse the skin capacitance discharges through the skin resistance instead, and no current flows through the limb; notice, however, the lengthy relaxation of the stimulus voltage in this case. The interface impedance increases during the recording session as the paste is depleted of charge conductors, and over the lifetime of the electrodes as their effective surface area is reduced by corrosion.

A simple model for the high-current-density electrode interface which ignores half-cell and galvanic potentials consists of a nonlinear resistor in parallel with a fixed capacitor. Stephens [11] and Barker [5] have empirically modeled the resistance by the relationship $I = aV + bV^2$ and analytically derived relaxations such as those in Fig. 2.

C. Subcutaneous Tissue

The dermis and underlying tissues and fluids can be modeled as a purely resistive volume conductor [1], [3], [4], [14].

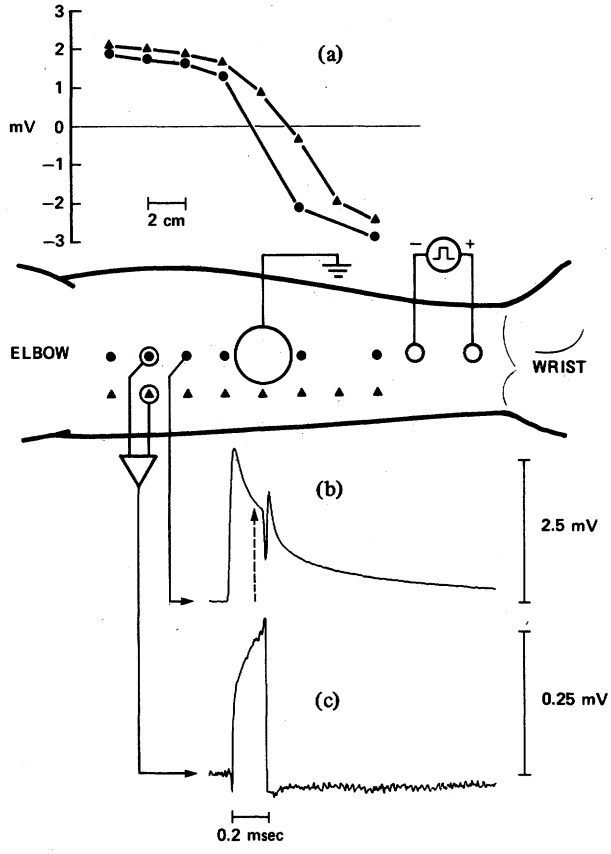

Fig. 3. Potential field in the arm generated by the stimulus current. (a) Voltages measured at several points on the limb during the stimulus pulse. (b) Waveform of the voltage at one point. (The arrow indicates the time at which the voltages in (a) were measured.) (c) Illustration of the differential voltage between two points not on an equipotential line.

The resistance between any two points is affected by the shape of the limb and the location of bone, tendon, and blood vessels, but is usually small—100-500 Ω. The current injected between the stimulating electrodes flows throughout the limb and sets up a potential field. The spatial variation of this field is illustrated in Fig. 3(a), which shows voltages measured with respect to ground at several points on the arm in response to a constant-current pulse of 5 mA. Notice that the potentials in the limb are small compared to the stimulus voltage, most of which is dropped across the impedances of the stimulating electrodes.

The waveform of the potential at one point on the limb is shown in Fig. 3(b). The waveform consists of two components: the potential generated by the stimulus current, which varies from point to point on the limb, and the voltage dropped by the escape current across the ground electrode impedance. These two components will be further discussed in the section on common-mode conversion.

D. Recording Amplifier

A good amplifier for surface electrode recording must have a high input impedance (10 MΩ) to record without distortion from electrodes with impedances of tens of kilohms, and a high common-mode rejection ratio (10^5) to effectively reject the common-mode voltage at the recording site (typically <0.2 V). Such an amplifier generally has an adjustable high-pass filter for restricting low-frequency noise due to slow half-cell and galvanic potential changes and amplifier drift, and an adjustable low-pass filter for restricting high-frequency thermal noise.

III. Sources of Artifact and Methods for its Reduction

The components described in the preceding section interact to produce artifact in four major ways. This section models these four sources of artifact. The models are not intended to enable accurate reconstruction of particular artifact signals since identification of component parameters is difficult. Rather, they are intended to provide insight into methods for artifact reduction and cancellation.

A. Voltage Gradients

A major source of artifact is the voltage difference V_D produced between the recording electrodes by current flowing through the limb [1], [2]. The stimulus current sets up a voltage gradient at the recording site which, as illustrated in Fig. 3(c), contributes to two artifact components: the pulse itself contributes to the spike, and the succeeding discharge of the stimulating electrodes through the limb contributes to the fast tail. The size of this gradient decreases as the distance between the stimulating and recording sites is increased. The escape current also flows through the limb, but it is small (<50 μA) and only affects the potential field between the stimulating and grounding sites.

V_D can be substantially reduced by positioning the two recording electrodes on an equipotential line. The equipotential lines, although approximately perpendicular to the midline as they cross it, soon curve toward the stimulating site. Fig. 3(a) suggests that an indifferent electrode 2 cm from the nerve at the elbow should be about 2 cm closer to the stimulating site than the on-nerve electrode is. Since the stimulating electrodes are not perfect point sources, but consist of regions of differing frequency-dependent impedance [10], the shape of the potential field in the limb is also frequency-dependent, and the equipotential lines shift slightly during the stimulus pulse. For this reason V_D cannot always be eliminated by careful placement of the recording electrodes.

The tail of V_D can be essentially eliminated by using a high-output-impedance (constant-current) stimulator. A constant-voltage stimulator can be converted into a constant-current stimulator by a simple circuit such as that described in [15].

B. Common-Mode Conversion

The common-mode voltage at the recording site (V_{CM}) is converted to an artifact signal proportional in amplitude to the imbalance between the recording electrode impedances. The Laplace transform of the converted signal is given by

$$V_{CCM}(s) = \frac{Z_1 - Z_2}{Z_I} V_{CM}(s)$$

where Z_1 and Z_2 are the recording electrode impedances and Z_I is the recording amplifier's input impedance. $Z_1 - Z_2$ is rarely as much as 10 kΩ, and can be reduced by scrubbing the skin well under each electrode.

V_{CM} is the sum of the voltage difference V_{GR} dropped between the grounding and recording sites by the stimulus cur-

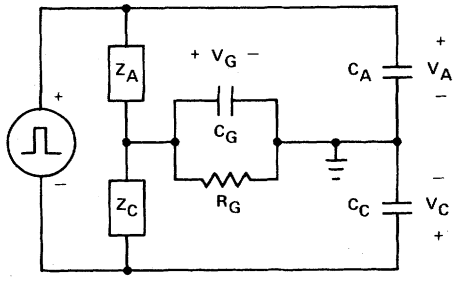

Fig. 4. Model of the ground electrode voltage (V_G) for a transformer coupled stimulator.

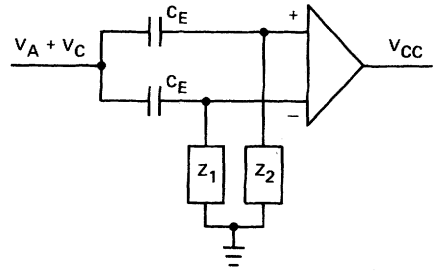

Fig. 5. Model of the capacitive coupling between the stimulating and recording leads.

rent, and the voltage V_G dropped across the ground electrode by the escape current [2]. The first term can be reduced by positioning the ground electrode close to the recording site (2-5 cm distal to it), rather than midway between the recording and stimulating sites where it is commonly placed.

At the rising and falling edges of the stimulus pulse, the stray stimulator capacitances must be charged and discharged. Unless the capacitances and the stimulating electrode impedances are perfectly balanced, this results in current flow through the ground electrode [1], [2]. This current is called the escape current. If the stray capacitances can be modeled as lumped capacitors at the stimulator outputs, then the voltage dropped by the escape current across the ground electrode is given by (see Fig. 4)

$$V_G(s) = \frac{-s[V_A(s)\,C_A + V_C(s)\,C_C]\,R_G}{1 + sR_GC_G}$$

where V_A and V_C are the anode and cathode voltages, C_A and C_C are the capacitances between the stimulator outputs and ground, R_G and C_G are the resistance and capacitance of the ground electrode, and the subcutaneous tissue is approximated as a perfect conductor. For a constant-current stimulator, the driving term is a nonlinear function of $V_AC_A + V_CC_C$. In either case, the amplitude of V_G can be reduced by using a large ground electrode to increase C_G, and its time course can be shortened by scrubbing the skin under the ground electrode to reduce R_G.

C. Capacitive Coupling

The third source of artifact is the capacitive coupling between the stimulating and recording leads. These leads are usually not shielded in order to minimize their capacitance to ground, and as a result, the capacitance between them in a normal configuration is about 0.5 pF even when care is taken to keep them far apart. Since each pair of leads runs together, the capacitance between each stimulating and recording lead is approximately the same (C_E). In this case, the coupled signal depends on the imbalance between recording electrode impedances as follows (see Fig. 5):

$$V_{CC}(s) = sC_E(Z_1 - Z_2)\,[V_A(s) + V_C(s)].$$

In this model the subcutaneous tissue is approximated as a perfect conductor connected to ground. The driving term $V_A + V_C$ depends on the imbalance between stimulating electrode impedances. The anode usually goes more positive during the stimulus pulse than the cathode goes negative, so that a net positive voltage drives the recording leads. Scrubbing the skin helps equalize the impedances, and electrodes which have become greatly imbalanced by corrosion should be replaced.

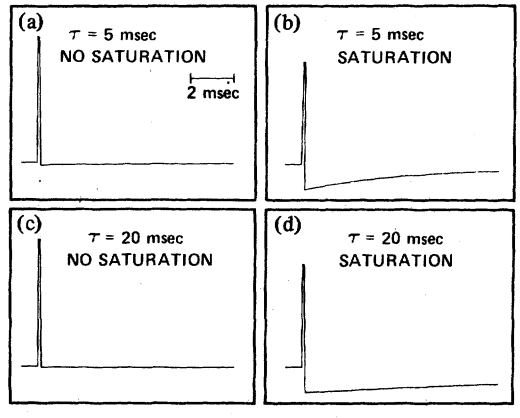

Fig. 6. Effects of the recording amplifier's high-pass filter time constant (τ) and of amplifier saturation.

D. Shaping by the Recording Amplifier

The passage of the spike through the recording amplifier's high-pass filter introduces a slow exponential tail into the signal [16], [20], as illustrated in Fig. 6(a) and (c). If the spike is large enough to saturate the amplifier, a more severe distortion may occur [Fig. 6(b) and (d)], and if saturation occurs in an early stage of amplification, recovery from the overload may take several milliseconds. The spike can usually be kept small enough to prevent saturation by careful positioning of the recording electrodes. The amplitude of the exponential tail can be further reduced by decreasing the amplifier's high-pass cutoff [compare Fig. 6(a) and (c)]. Several investigators [16]-[20] have also suggested simple circuits for blocking the amplifier during the stimulus pulse to prevent generation of the tail and to protect against overload.

E. Summary

The methodological rules for reducing artifact can be summarized as follows.

1) Scrub the skin well under each electrode (several vigorous rubs with a swab dipped in pumice paste so that the skin is reddened) and use electrolyte paste. This assures consistent, low-impedance contacts.

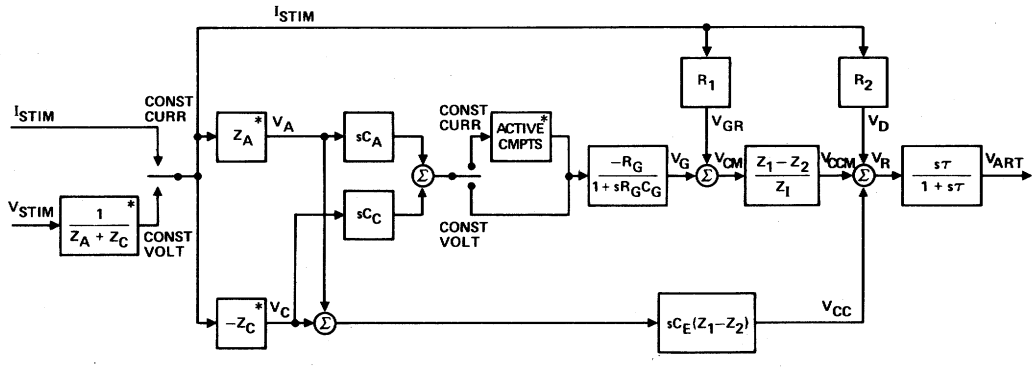

Fig. 7. Block diagram of the sources of artifact. The blocks marked with an asterisk are nonlinear.

2) Use constant-current stimulation to prevent the stimulating electrodes from discharging through the limb.

3) Place the recording electrodes on an equipotential line. The orientations of the equipotential lines depend on the stimulation configuration and on inhomogeneities in the limb. The indifferent electrode can be attached to a wand to facilitate probing for the optimal position.

4) Use a large ground electrode and place it near the recording site. This reduces both components of the common-mode voltage at the recording site.

5) Keep the stimulating and recording leads short and far apart to minimize capacitive coupling between them.

6) Replace well-used stimulating electrodes, especially if they show pronounced discoloration. Imbalanced stimulating electrodes contribute to capacitively coupled artifact.

7) Set the recording amplifier's high-pass cutoff as low as is practical to reduce the amplitude of the artifact's slow tail. The amplifier can be blocked during the stimulus pulse by a circuit such as described in [16]-[20] if necessary.

The sources of artifact are summarized in the block diagram of Fig. 7. The principal driving function is the stimulus current I_{stim}. If constant-voltage stimulation is used, I_{stim} is a nonlinear function of the stimulus voltage (V_{stim}). A signal proportional to I_{stim} is recorded differentially (V_D). Another signal proportional to I_{stim} is dropped between the grounding and recording sites (V_{GR}) and contributes to the common-mode voltage (V_{CM}). The stimulating electrode impedances nonlinearly filter I_{stim} to produce the pair of stimulating electrode voltages (V_A and V_C). This pair determines the escape current and hence the ground electrode voltage (V_G), which contributes to V_{CM}, and the capacitively coupled voltage (V_{CC}). The sum of V_D, V_{CC}, and the converted V_{CM} is recorded (V_R) and filtered by the recording amplifier to produce the final artifact (V_{art}).

IV. Signal Processing Methods for Artifact Cancellation

The rules presented in the preceding section cannot always eliminate artifact, especially when the nerve signal is weak or the limb is short. The artifact which remains must be removed by processing the recorded signal. Two components are easily removed: the spike does not ordinarily overlap the CAP and can be ignored, and the exponential tail introduced by the recording amplifier can be eliminated by inverse filtering. We have investigated three methods for cancelling the artifact which still remains by means of a separately recorded signal which is related to the artifact, but free of CAP. The inverse filtering and the three cancellation methods are described in this section.

The signal processing to be described was performed on a PDP 11/34 computer. The signals were digitized at the rate of 25 000 samples/s, beginning about 1 ms prior to the stimulus to provide a baseline. Between 32 and 512 records were digitally averaged, depending on the signal-to-noise ratio. The records shown in Figs. 8-10 have all been inverse filtered.

A. Inverse Filtering

The distortion introduced by the recording amplifier's high-pass filter is usually small, but it can be removed by passing the distorted signal through an inverse filter. For example, the discrete-time inverse filter for a single-pole high-pass filter with time constant τ is

$$V_R(t) = V_{\text{art}}(t) + \frac{1}{\tau} \sum_{k=0}^{t} V_{\text{art}}(k)\, \Delta t$$

where $V_{\text{art}}(t)$ is the averaged distorted signal and $V_R(t)$ is the reconstructed signal. Notice that the sampling rate of 25 kHz does not adequately sample the brief spike. As a result, $V_R(t)$ is inaccurate in the unimportant region of the spike, but suffers only a baseline change in the region of the CAP. The slow random variations which were attenuated by the high-pass filter have been averaged out of V_{art} and so are not reintroduced by inverse filtering.

B. Subthreshold Method

One way to obtain a CAP-free artifact signal is to reduce the stimulus intensity below the threshold for nerve excitation (typically <10 mA) [27]. In this method the same electrode configuration is used to record the purely artifactual subthreshold signal (V_{ST}) and the contaminated CAP signal (V_R). If the stimulating electrodes behaved linearly, V_{ST} could be scaled to perfectly cancel the artifact in V_R. In fact, the two artifact waveforms often have approximately the same shape,

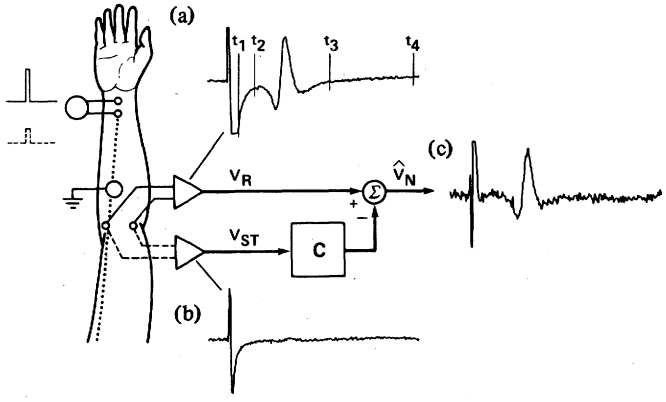

Fig. 8. Subthreshold method of artifact cancellation.

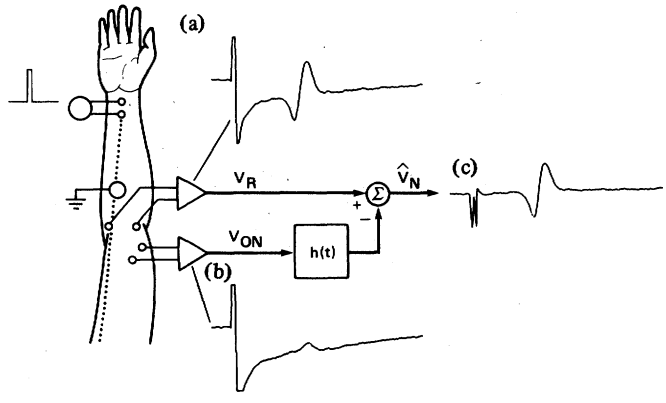

Fig. 9. Off-nerve method of artifact cancellation.

and fair cancellation is obtained in the following estimate of the CAP.

$$\hat{V}_N = V_R(t) - CV_{ST}(t)$$

where the scale factor C is computed as follows.

$$C = \frac{\sum_{k=t_1}^{t_2} V_R(k)\, V_{ST}(k) + \sum_{k=t_3}^{t_4} V_R(k)\, V_{ST}(k)}{\sum_{k=t_1}^{t_2} V_{ST}^2(k) + \sum_{k=t_3}^{t_4} V_{ST}^2(k)}.$$

Here (t_1, t_2) and (t_3, t_4) are chosen as shown in Fig. 8(a) to exclude the spike and CAP regions of the waveforms so that C will not be affected by the inaccurately sampled spike or biased to cancel any of the CAP signal.

An example of this method is shown in Fig. 8. Trace (a) is the contaminated CAP (V_R) and trace (b) is the subthreshold artifact (V_{ST}). The latter trace was multiplied by the scale factor computed as above and then subtracted from trace (a) to yield the estimate of the CAP ($\hat{V}_N$) shown in trace (c).

Notice that the subthreshold signal is very small; many responses were required to average out the noise. Fortunately, the threshold stimulus is not felt by the subject, and responses can be collected rapidly. The noise in the subthreshold signal is accentuated by scaling, as seen in Fig. 8(c), and smoothing of the resultant signal may be necessary.

C. Off-Nerve Method

In this method a second pair of recording electrodes is positioned away from the nerve to record a purely artifactual signal (V_{ON}) along with the contaminated CAP (V_R). Notice that even though the artifact signals in the two recording channels are both responses to the same stimulus pulse, according to the model in Fig. 7 they may not be linearly related. We assume, however, that an approximate linear relationship can be found between them, and estimate the CAP as follows.

$$\hat{V}_N(t) = \sum_{k=0}^{K} h(k)\, V_{ON}(t-k)$$

where the weighting function $h(k)$ is computed by the method of least-squares [21] as follows.

$$\begin{bmatrix} h(0) \\ \vdots \\ h(K) \end{bmatrix} = [A'A]^{-1}A' \begin{bmatrix} V_R(t_1) \\ \vdots \\ V_R(t_2 - K) \\ \hline V_R(t_3 + K) \\ \vdots \\ V_R(t_4) \end{bmatrix}$$

$$A = \begin{bmatrix} V_{ON}(t_1) & \cdots & V_{ON}(t_1 + K) \\ \vdots & & \vdots \\ V_{ON}(t_2 - K) & \cdots & V_{ON}(t_2) \\ \hline V_{ON}(t_3) & \cdots & V_{ON}(t_3 + K) \\ \vdots & & \vdots \\ V_{ON}(t_4 - K) & \cdots & V_{ON}(t_4) \end{bmatrix}.$$

t_1–t_4 are chosen as in the subthreshold method to exclude the spike and CAP regions of the waveforms, and K is typically between 0 and 10. Note that when $K = 0$, A is a scalar as in the subthreshold method.

An example of this method is shown in Fig. 9. Traces (a) and (b) show a contaminated CAP (V_R) and an off-nerve artifact (V_{ON}). The weighting function $h(k)$ was computed as above and convolved with trace (b), and then the result of this convolution was subtracted from trace (a) to yield the estimate of the CAP ($\hat{V}_N$) shown in trace (c).

One major disadvantage of this method is the difficulty of finding a location for the second recording pair which is completely free of CAP signal. Notice the small nerve signal present in Fig. 9(b).

D. Double-Stimulus Method

We have also considered a method proposed by Barker [5] in which a second stimulus pulse is applied to the nerve during its refractory period. The refractory period is the period immediately following the initiation of a CAP (and lasting about 0.6 ms in the median nerve [22]) during which a second stimulus fails to evoke a second nerve response. Thus, the first pulse evokes both artifact and CAP, the second pulse evokes only artifact. Assuming that the double-pulse artifact is the linear superposition of two single-pulse artifacts, the signal

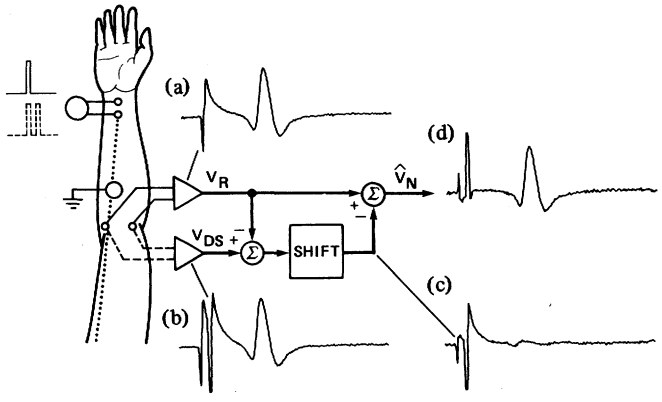

Fig. 10. Double-stimulus method of artifact cancellation.

evoked by the double stimulus (V_{DS}) can be used to cancel the artifact from a normally evoked CAP (V_R) as follows.

$$\hat{V}_N(t) = V_R(t) - [V_{DS}(t+T) - V_R(t+T)]$$

where T is the interval between the double stimuli.

An example of this method is shown in Fig. 10. Traces (a) and (b) show the responses to a single stimulus (V_R) and to double stimuli 0.4 ms apart (V_{DS}). These two signals were subtracted to yield an estimate of the single-pulse artifact [trace (c)], which was then aligned with and subtracted from trace (a) to yield the estimate of the CAP ($\hat{V}_N$) shown in trace (d).

V. Discussion

Stimulators and electrodes other than those described in this paper are also used in nerve-conduction studies. Biphasic stimulus pulses are used because they quickly discharge the stimulating electrodes, thus reducing stimulus artifact [23], and because they transfer no net charge across the stimulating electrode interfaces, thus prolonging electrode life. However, biphasic pulses are more difficult to generate and do not activate the nerve as sharply as monophasic pulses [24]. Silver/silver chloride electrodes are used because of their low metal/electrolyte impedance and their low half-cell potential drift, but they require frequent replating, and their overall interface impedance is still dominated by the impedance of the skin. We have found little reduction in artifact when stainless steel electrodes were replaced by silver/silver chloride ones. Platinum alloy needle electrodes pierce the skin and provide direct, low-impedance contact with the subcutaneous tissue, typically 2 kΩ in parallel with 20 μF. Considerably less voltage is required to excite the nerve when needle stimulating electrodes are used, reducing the capacitively coupled and common-mode artifact components, but we have found that scrubbing the skin well under surface electrodes reduces artifact to a comparable degree. In addition, needle electrodes are invasive, must be sterilized before each use, require careful insertion, and are not as well tolerated by all subjects.

Even a small amount of artifact can seriously impair analysis which tries to extract a great deal of information from the CAP waveform. This problem is illustrated in Fig. 11. Fig. 11(a) shows an artifact-free CAP and the distribution of conduction velocities (DCV) computed using it by the method of Cummins *et al.* [25], [26]. To demonstrate the effect of

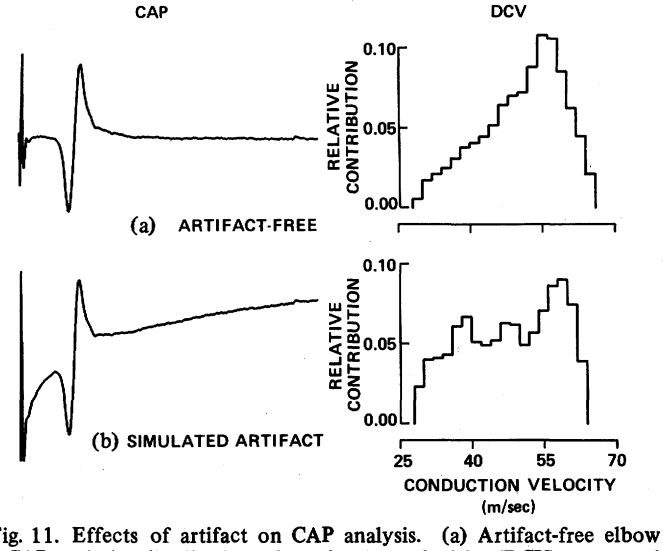

Fig. 11. Effects of artifact on CAP analysis. (a) Artifact-free elbow CAP and the distribution of conduction velocities (DCV) computed using it. (b) CAP from (a) superimposed on a simulated artifact tail and the erroneous DCV computed using it.

artifact, an exponential was added to the CAP to yield the waveform shown in Fig. 11(b). The DCV computed using this contaminated waveform is also shown in Fig. 11(b) and bears little resemblance to the true DCV.

The artifact components which arise from the voltage gradients, the common-mode voltage, and the capacitive coupling have similar shapes and durations and vary considerably in size from one recording session to another. As a result, it is often difficult to judge their relative sizes or even to tell which predominates. We have found that each component is usually reduced to an acceptable level by following the rules summarized in Section III. When unacceptable artifact persists, we have found the cancellation methods presented in this paper to be useful, although each method has its drawbacks, and we do not yet have enough experience to know which will work best in a given situation. An alternative method, proposed by Kovacs [28], which fits the artifact by a function of the empirically derived form $A(1 - at)\exp(-at)$, has proved successful in cancelling artifact from clinically measured median and ulnar nerve responses.

It is worthwhile to examine the cancellation methods in light of the model presented in Fig. 7 to see how they are affected by the nonlinearities involved in the generation of the artifact. Notice first of all that the nonlinearities are associated with the stimulator and the stimulating electrodes. These give rise to signals which drive the linear transfer functions of the recording electrodes and amplifier.

The subthreshold method uses the same electrode configuration to record the CAP and the subthreshold signal, and assumes proportionality of the driving functions at the two stimulus intensities. With constant-current stimulation, I_{stim} is proportional, but V_A and V_C are not (see Fig. 2); and so this method will perform well if the predominant artifact component is V_D or V_{GR}, but will not perform well if V_G or V_{CC} predominates or if several components are large. With constant-voltage stimulation none of the driving functions are proportional and the method will not perform well.

The off-nerve method uses the same stimulus to evoke both the CAP and the off-nerve signal, and so the driving functions I_{stim}, V_G, and $V_A + V_C$ are the same for both recording channels. The transfer functions of the two recording channels differ, but a linear relationship exists between them. If the two recording sites are near one another, so that they feel the same capacitive coupling to the stimulating leads and the same common-mode voltage, and if the tail of V_D is negligible (as it is with constant-current stimulation), then the artifacts recorded by the two channels will also be linearly related. The least-squares method will identify this relationship and effectively cancel the artifact in the on-nerve channel.

The double-stimulus method uses both the same stimulus intensity and the same electrode configuration to evoke and record the CAP and the double-stimulus signal. Since the stimulating electrodes are nonlinear, however, the two pulses of the double stimulus superimpose nonlinearly. As a result, the driving functions generated by the second pulse, and hence the second artifact, may differ considerably from those generated by the first pulse.

The impedances of the stimulating and recording electrodes and the capacitance between them can change during a recording session as sweating, drying of the electrolyte paste, and movement of the limb take place. For this reason the CAP and the auxiliary signal should be recorded close together in time with care taken not to disturb the configuration between recordings. A programmable stimulator which would alternate between normal and subthreshold stimuli or single and double stimuli would allow both signals to be recorded simultaneously, as they are in the off-nerve method.

Computationally, the double-stimulus method is the simplest, requiring only subtraction and shifting. The subthreshold method requires multiplication as well. Most complicated is the off-nerve method which must solve the least-squares algorithm. Any of the methods is simple enough to be implemented, along with the necessary data sampling and averaging functions, on a microprocessor-based system.

References

[1] C. Guld, "The reduction of stimulus interference in electrophysiology," in *Proc. 3rd Int. Conf. Med. Electron.*, part 1, 1960, pp. 103–105.

[2] J. M. M. Neilson, "An investigation of methods of recording the electrical activity of the nervous system with particular reference to the occurrence and suppression of stimulus artefact," dissertation, University of Edinburgh, Scotland, 1962.

[3] R. D. Gatzke, "The electrode: A measurement systems viewpoint," in *Biomedical Electrode Technology*, H. A. Miller and D. C. Harrison, Eds. New York: Academic, 1974.

[4] D. K. Swanson and J. G. Webster, "A model for skin-electrode impedance," in *Biomedical Electrode Technology*, H. A. Miller and D. C. Harrison, Eds. New York: Academic, 1974.

[5] A. T. Barker, "Determination of the distribution of conduction velocities in human nerve trunks," dissertation, Sheffield Univ., Sheffield, England, 1974.

[6] D. A. Robinson, "The electrical properties of metal microelectrodes," *Proc. IEEE*, vol. 56, pp. 1065–1071, 1968.

[7] D. Jaron, S. A. Briller, H. P. Schwan, and D. B. Geselowitz, "Nonlinearity of cardiac pacemaker electrodes," *IEEE Trans. Biomed. Eng.*, vol. BME-16, pp. 132–138, 1969.

[8] L. A. Geddes, *Electrodes and the Measurement of Bioelectric Events.* New York: Wiley-Interscience, 1972.

[9] —, "Interface design for bioelectric systems," *IEEE Spectrum*, vol. 9, pp. 41–48, Oct. 1972.

[10] A. M. Dymond, "Characteristics of the metal-tissue interface of stimulation electrodes," *IEEE Trans. Biomed. Eng.*, vol. BME-23, pp. 274–280, 1976.

[11] W. G. S. Stephens, "The current-voltage relationship in human skin," *Med. Electron. Biol. Eng.*, vol. 1, pp. 389–399, 1963.

[12] R. Edelberg, "Electrical properties of the skin," in *Methods in Psychobiology*, C. C. Brown, Ed. Baltimore, MD: Williams & Wilkins, 1967.

[13] H. R. Elden, *Biophysical Properties of the Skin*, vol. 1. New York: Wiley, 1971.

[14] R. Plonsey, *Bioelectric Phenomena.* New York: McGraw-Hill, 1969.

[15] K. L. Cummins, "A simple circuit to convert a constant-voltage stimulator into a constant-current stimulator," to be published.

[16] V. O. Andersen and F. Buchthal, "Low noise alternating current amplifier and compensator to reduce stimulus artefact," *Med. Biol. Eng.*, vol. 8, pp. 501–508, 1970.

[17] J. A. Freeman, "An electronic stimulus artifact suppressor," *Electroenceph. Clin. Neurophysiol.*, vol. 31, pp. 170–172, 1971.

[18] R. J. Roby and E. Lettich, "A simplified circuit for stimulus artifact suppression," *Electroenceph. Clin. Neurophysiol.*, vol. 39, pp. 85–87, 1975.

[19] T. L. Babb, E. Mariani, G. M. Strain, J. P. Lieb, H. V. Soper, and P. Crandall, "A sample and hold amplifier system for stimulus artifact suppression," *Electroenceph. Clin. Neurophysiol.*, vol. 44, pp. 528–531, 1978.

[20] D. D. Walker and J. Kimura, "A fast-recovery electrode amplifier for electrophysiology," *Electroenceph. Clin. Neurophysiol.*, vol. 45, pp. 789–792, 1978.

[21] D. Luenberger, *Optimization by Vector Space Methods.* New York: Wiley, 1969.

[22] R. W. Gilliatt and R. G. Willison, "The refractory and supernormal periods of the human median nerve," *J. Neurol. Neurosurg. Psychiat.*, vol. 26, pp. 136–147, 1963.

[23] H. J. Spencer, "An automatic, optically isolated, biphasic constant current stimulator adapter for artefact suppression," *Electroenceph. Clin. Neurophysiol.*, vol. 51, pp. 215–217, 1981.

[24] P. H. Gorman, J. T. Mortimer, and C. van der Honert, "Enhancing excitability differences between nerve fibers," in *Proc. Annu. Conf. Eng. Med. Biol.*, vol. 33, 1980, p. 63.

[25] K. L. Cummins, L. J. Dorfman, and D. H. Perkel, "Nerve-fiber conduction velocity distributions. II. Estimation based on two compound action potentials," *Electroenceph. Clin. Neurophysiol.*, vol. 46, pp. 647–658, 1979.

[26] —, "Nerve conduction velocity distributions: A method for estimation based upon two compound action potentials," in *Conduction Velocity Distributions: A Population Approach to Electrophysiology of Nerve*, L. J. Dorfman, K. L. Cummins, and L. J. Leifer, Eds. New York: Liss, 1981.

[27] Z. L. Kovacs, "The estimation of the distribution of conduction velocities in intact peripheral nerves," M.I.T., Cambridge, MA, Tech. Rep. ESL-870, 1977.

[28] —, "Filtering the stimulus artifact in recordings from nerves," in *Proc. Annu. Conf. Eng. Med. Biol.*, vol. 31, 1978, p. 269.

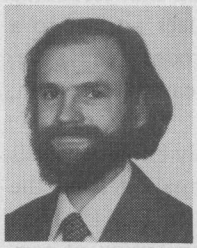

Kevin C. McGill was born in Indianapolis, IN, on June 19, 1952. He received the A.B., B.S.E.E., and M.S.E.E. degrees from the University of Notre Dame, Notre Dame, IN, in 1974, 1975, and 1979, respectively.

From 1976 to 1978 he was with Naval Avionics Center in Indianapolis. He is currently a Ph.D. candidate in electrical engineering at Stanford University, Stanford, CA, and a Research Assistant in the Department of Neurology at Stanford University Medical Center. His research interests are in biological signal processing.

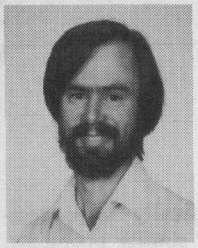

Kenneth L. Cummins (S'73–M'78) was born in Glendale, CA, on October 2, 1948. He received the B.S. degree in engineering from the University of California, Irvine, in 1974, and the M.S. and Ph.D. degrees in electrical engineering from Stanford University, Stanford, CA, in 1975 and 1978, respectively.

In 1978–1979 he was a Postdoctoral Research Fellow with the Neurology Department, Stanford University Medical Center, where he performed research in clinical electrophysiology, including methods developed in his Ph.D. dissertation. He is currently with the Rehabilitative Engineering Research and Development (RERanD) Center, Palo Alto Veterans Administration Medical Center, Palo Alto, CA. He holds a joint appointment as Lecturer at Stanford University Medical Center. His current research interests include biological modeling, applications of signal processing to neurology and neurophysiology, and sensory aids.

Dr. Cummins is a member of Eta Kappa Nu, Society for Neuroscience, and the IEEE Engineering in Medicine and Biology Society.

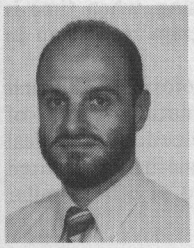

Leslie J. Dorfman was born in Montreal, P.Q., Canada, on September 11, 1943. He received the B.Sc. degree in experimental psychology from McGill University, Montreal in 1964, and the M.D. degree from Albert Einstein College of Medicine, Bronx, NY, in 1968.

He took residency training in internal medicine at Greenwich Hospital, Greenwich, CT and in neurology at Stanford University Medical Center, Stanford, CA; and fellowship training in electromyography at the National Hospital for Neurological Diseases, Queen Square, London, England. Since 1974 he has been on the faculty of Stanford University School of Medicine, where he is currently Associate Professor of Neurology and Director of the Laboratories of Electromyography and Sensory Evoked Potentials. His research interest is the application of signal processing techniques to clinical neurophysiological data for diagnosis of neurological disorders.

Bruno B. Berlizot was born in Toulon, France, on August 23, 1956. He received the Ingénieur Diploma from Ecole Nationale Supérieure de Physique, Marseilles, France, in 1979 and the M.S. degree in electrical engineering from Stanford University, Stanford, CA, in 1980.

He is one of the founders of Services Informatiques Logiciels et Etudes-Siloé in Saint-Tropez, France. Currently, he is the technical manager of Siloé. His research interests include microcomputers and real-time applications.

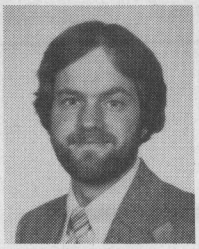

Kelly Luetkemeyer was born on November 28, 1956, in Tuscumbia, MO. He received the A.B. degree (honors) in mathematics and computer science from the University of Missouri, Columbia, in 1979 and the M.S.E.E. degree from Stanford University, Stanford, CA, in 1981.

From 1979 to the present he has been employed by NASA at Ames Research Center. At NASA he is involved with three-dimensional computer graphics to represent fluid dynamics flow field solutions. He has also designed computer models of biological molecules. His research interests are in computer graphics and image processing of biological systems.

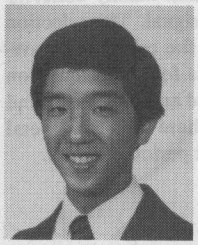

Dwight G. Nishimura was born in Honolulu, HI, on January 31, 1959. He received the B.S. and M.S. degrees in electrical engineering from Stanford University, Stanford, CA, in 1980.

He is currently a Ph.D. candidate in electrical engineering at Stanford University where he works as a National Science Foundation Graduate Fellow in the Information Systems Laboratory, Department of Electrical Engineering. His research interests are in medical imaging, image processing, and estimation theory.

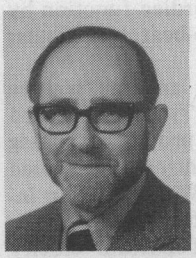

Bernard Widrow (M'58–SM'75–F'76) was born in Norwich, CT, on December 24, 1929. He received the B.S., M.S., and Sc.D. degrees from the Massachusetts Institute of Technology, Cambridge, in 1951, 1953, and 1956, respectively.

From 1951 to 1956, he was a Staff Member of the M.I.T. Lincoln Laboratory and a Research Assistant in the Department of Electrical Engineering of M.I.T. He joined the M.I.T. faculty in 1956 and taught classes in radar, theory of sampled-data systems, and control theory. In 1959 he joined the faculty of Stanford University, Stanford, CA, and is now Professor of Electrical Engineering. He is presently engaged in research and teaching in systems theory, pattern recognition, adaptive filtering, and adaptive control systems. He is Associate Editor of *Information Sciences* and *Pattern Recognition*.

Dr. Widrow is a member of the American Association of University Professors, the Pattern Recognition Society, Sigma Xi, and Tau Beta Pi, and is a Fellow of the American Association for the Advancement of Science.